The AAPS Journal (2025) 27:7
https://doi.org/10.1208/s12248-024-00997-5

RESEARCH ARTICLE

Tumor-Infiltration Mimicking Model of Contaminated Ovarian Tissue as an Innovative Platform for Advanced Cancer Research

Saeid Moghassemi[1] · Arezoo Dadashzadeh[1] · Carolina M. Lucci[2] · Christiani A. Amorim[1]

Received: 10 September 2024 / Accepted: 9 November 2024

Abstract

The development of advanced preclinical models is crucial for the evaluation and validation of novel therapeutic strategies in oncology. Three-dimensional (3D) microtumor models, which incorporate both cancer and stromal cells within biomimetic hydrogels, have emerged as powerful tools that more accurately replicate the complex tumor microenvironment compared to traditional two-dimensional (2D) cell culture systems. In this context, our study aims to develop 3D microtumor models by integrating cancer and stromal cells within an extracellular-matrix-mimetic hydrogel, as a physiologically accurate microtumor model that can serve as an innovative platform for advanced cancer research and drug screening. Microtumors composed of varying ratios of leukemia cells (HL-60) to healthy ovarian stromal cells (SCs) (1:1, 1:10, 1:100, or 1:1000) were encapsulated in PEGylated fibrin hydrogel and cultured for 5 days. The proliferation and dynamics of cancerous and healthy cell populations were evaluated using CD43/Ki67 immunofluorescence double staining. Our findings indicate that tumor development and malignancy progression can be influenced by adjusting cell culture ratios and incubation time. Notably, the HL-60:SCs ratio of 1:100 closely replicated leukemia cell invasion in ovarian tissue, demonstrating detectable malignancy on the third and fifth days without significant changes in total cell density dynamics. This 3D leukemia microtumor model offers superior physiological relevance compared to traditional 2D *in vitro* assays and shows promising potential for applications in cellular analysis and drug screening.

Keywords 3D scaffold · hydrogel · PEGylated Fibrin · tissue engineering · tumor model

Introduction

Although animal models may provide physiological structures simulating human tissue and organs, they are costly, and their application is constrained by feasibility and ethical concerns regarding the 3R rules (Refinement, Reduction, and Replacement) (1). As an alternative, two-dimensional (2D) cell culture models have long been the standard in preclinical cancer research and drug testing (2). However, these 2D models fail to replicate the complexity of *in vivo* tumors, particularly the tumor microenvironment (TME), which involves gradients in pH, nutrients, and metabolites, as well as intricate 3D architectures that govern cell–cell and cell–matrix interactions (3, 4). This leads to a significant gap between the data obtained from 2D cultures and the actual *in vivo* responses, reducing the predictive power of these models for drug efficacy.

Over the past decade, there has been a substantial shift towards the development and application of 3D culture systems that more accurately represent the structural and biological features of tumors (4). These 3D models have demonstrated improved relevance for studying cancer cell behavior, invasion, and therapeutic responses by providing a more physiologically relevant environment (5, 6). Moreover, the interactions between various cell types significantly influence their behavior in TME, contrasting with their independent culture (7). For instance, acute myeloid leukemia (AML) cells, known for their heightened levels of reactive oxygen species (ROS), exhibit decreased ROS and acetate secretion levels when co-cultured with stromal cells (SCs) compared to when cultured in isolation (8). This occurrence

✉ Christiani A. Amorim
christiani.amorim@uclouvain.be

[1] Pôle de Recherche en Physiopathologie de La Reproduction, Institut de Recherche Expérimentale Et Clinique, Université Catholique de Louvain, Avenue Hippocrate 54, Bte B1.55.03, 1200 Brussels, Belgium

[2] Department of Physiological Sciences, Institute of Biological Sciences, University of Brasília, Brasília, Brazil

Published online: 25 November 2024

may be ascribed to the upregulation of several gap junction genes in SCs during co-culture, potentially affecting ROS transfer (9). Therefore, biomimetic 3D microtumors may be an appropriate "connecting bridge" between tailored 2D *in vitro* and animal *in vivo* studies, which can decrease laboratory animal usage (10).

Among the various biomaterials used for 3D tumor modeling, PEGylated fibrin hydrogels have emerged as promising candidates as they offer the added benefit of simulating critical aspects of the TME, including cell–cell and cell–matrix interactions, which are vital for studying tumor invasion and metastasis. Polyethylene glycol (PEG) provides mechanical tunability, biocompatibility, and resistance to protein adhesion. On the other hand, fibrin, a natural component of the extracellular matrix, plays an essential role in tumor progression by promoting angiogenesis and serving as a supportive matrix for invading cancer cells (11). By combining PEG and fibrin, it is possible to create scaffolds that mimic the native tissue environment while providing a platform for controlled manipulation of mechanical properties, enabling the study of tumor mechanics and cell behavior in a biomimetic setting. Indeed, recent research has shown the effectiveness of PEGylated fibrin scaffolds in developing 3D tumor models, which allow for the study of how the 3D microenvironment influences cancer cell growth (12). This 3D matrix has been found to support tumor growth in a manner that closely resembles *in vivo* conditions (11). Moreover, it can be tailored to mimic the mechanical and biological properties of specific tissues, offering advantages over other biomaterials by supporting both structural integrity and cell functionality.

Our research builds on this foundation by utilizing a PEGylated fibrin hydrogel formulation designed to mimic the biomechanical properties of ovarian tissue. This scaffold, specifically engineered for ovarian tissue applications, provides an optimal platform for studying tumor invasion within ovarian environments. Compared to other PEGylated fibrin scaffolds, our formulation is tailored to replicate the mechanical properties of the human ovarian cortex, which is essential for preserving the physiological behavior of the embedded cells (13, 14). These properties allow the scaffold to support the co-culture of leukemia and stromal cells, offering a more accurate representation of the interactions within the ovarian TME. Ultimately, our goal is to develop strategies for purging ovarian tissue of cancer cells before autotransplantation (15–17), ensuring that fertility restoration methods for cancer patients are safe and effective.

In this study, we present a novel tumor-infiltration model (TM) using our PEGylated fibrin 3D scaffold to simulate the invasion of HL-60 leukemia cells into ovarian stromal cells. This co-culture model enables the investigation of leukemia cell behavior within a physiologically relevant ovarian tissue environment. By leveraging the biomechanical properties of the scaffold and its ability to sustain both cancer and stromal cells, our model provides a platform for advanced cancer research, including drug screening and the study of tumor-stromal interactions.

Materials and Methods

Materials

Human fibrinogen (F3879), thrombin (T7009), O,O′-Bis[2-(N-Succinimidyl-succinylamino)ethyl]polyethylene glycol (NHS-PEG-NHS; 2000 Da; 713783), $CaCl_2$ (C5080), Liberase DH (05401089001), Triton X-100 (X100), 80 µm (NY8002500), and 30 µm (NY3002500) nylon net filters, HL-60 cell line (98070106), Hoechst 33342 (14533), and trypan blue (T8154) were purchased from Sigma Aldrich (Belgium). Dulbecco's modified Eagle's medium F-12 nutrient mixture (21041–025, DMEM/F12), heat-inactivated fetal bovine serum (16140–071; HI FBS), antibiotics and antimycotic (15240–062; AA), RPMI-1640 medium (61870–010), Dulbecco's Phosphate Buffered Saline with Ca2 + and Mg2 + (14040–091, DPBS) (1x), and DNase (89836) were obtained from Gibco Life Technologies Ltd. normal goat serum (31872; NGS), Alexa FluorTM 488 goat anti-mouse IgG (A11001), Alexa FluorTM 594 goat anti-mouse IgG (A11005), TaqMan probes for sialophorin (Hs01872322-s1; SPN) and glyceraldehyde-3-phosphate dehydrogenase (Hs02758991_g1; GAPDH) were purchased from ThermoFisher Scientific Corp. (Belgium). Fluorescent mounting medium (S3023) and monoclonal anti-human Ki67 (M7240) were purchased from Dako (Glostrup, Denmark). Bovine serum albumin (3854.3; BSA), Histosafe, and CD43 antibody (1-CD160) were respectively purchased from Carl Roth (Germany), Yvsolab SA (Belgium), and Quartett GmbH. All other chemicals were of the highest grade commercially available.

Cell Isolation and Culture

From frozen-thawed human ovarian tissues, ovarian SCs were isolated, with authorization from the University Catholique de Louvain's Institutional Review Board (approved on May 13, 2019; IRB reference: 2012/23MAR/125, registration number B403201213872) (18, 19). After being mechanically broken down, the fragments were briefly washed in DPBS containing Ca^{2+} and Mg^{2+}, then enzymatically broken down using 0.28 Wünsch units/mL Liberase DH and 8 Kunitz units/mL DNase. PBS without Ca^{2+} and Mg^{2+} was mixed with HI FBS in an equal amount to inactivate the digestive enzymes. The suspension was then run through Millipore 80 m and 30 m nylon net filters to remove any remaining particles. The final suspension

was centrifuged at 500 g for 10 min, and the pellet was then resuspended in cell culture media (DMEM/F12) in a T75 culture flask, containing 10% HI FBS and 1% AA. On the other hand, using RPMI cell culture media (RPMI medium containing 2 mM Glutamine, 10% HI FBS, and 1% AA), the HL-60 cell line was cultivated in T75 culture flasks (NUNC Brand Products, Denmark).

PEGylated Fibrin Hydrogel Preparation

PEGylated fibrinogen with the PEG:Fib 10:1 molar ratio was prepared in the tailored concentration reported by Dadashzadeh *et al*. (Fig. 1a) (14, 18). Briefly, human fibrinogen powder was added to the prewarmed PBS at 37°C to achieve a concentration of 85 mg/ml. 5 mg/ml NHS-PEG-NHS solution was prepared in PBS, as well. Then, solutions were sterilized with a 0.2 mm syringe filter, and an equal volume of PEG was added to the fibrinogen. After 2 h incubation at 37°C, the PEGylated fibrinogen solution was diluted with PBS to reach 39.06 mg/ml. Moreover, 50.36 IU/ml of thrombin was obtained by reconstitution and dilution of human thrombin in 40 mM CaCl2. The hydrogel was produced by combining equal volumes of the PEGylated fibrinogen solution and thrombin, then incubating at 37°C for 15 min.

Hydrogel Microstructure and Surface Morphology

Scanning electron microscopy (SEM) was employed to evaluate the PEGylated fibrin hydrogel microstructure and surface morphology. After an overnight fixation in 4% paraformaldehyde, the hydrogel was rinsed with 0.1 M cacodylate buffer. Then, the sample was penetrated with glycerol in two stages: 15% for 30 min and 30% for the entire night. Afterward, a blade was used to freeze-fracture it after being quickly submerged in liquid nitrogen. A graded acetone series (50%, 70%, 80%, 90%, and three variations of 100%) was applied to the sample for 15 min at a time to dehydrate it. Following dehydration, the samples were processed in a

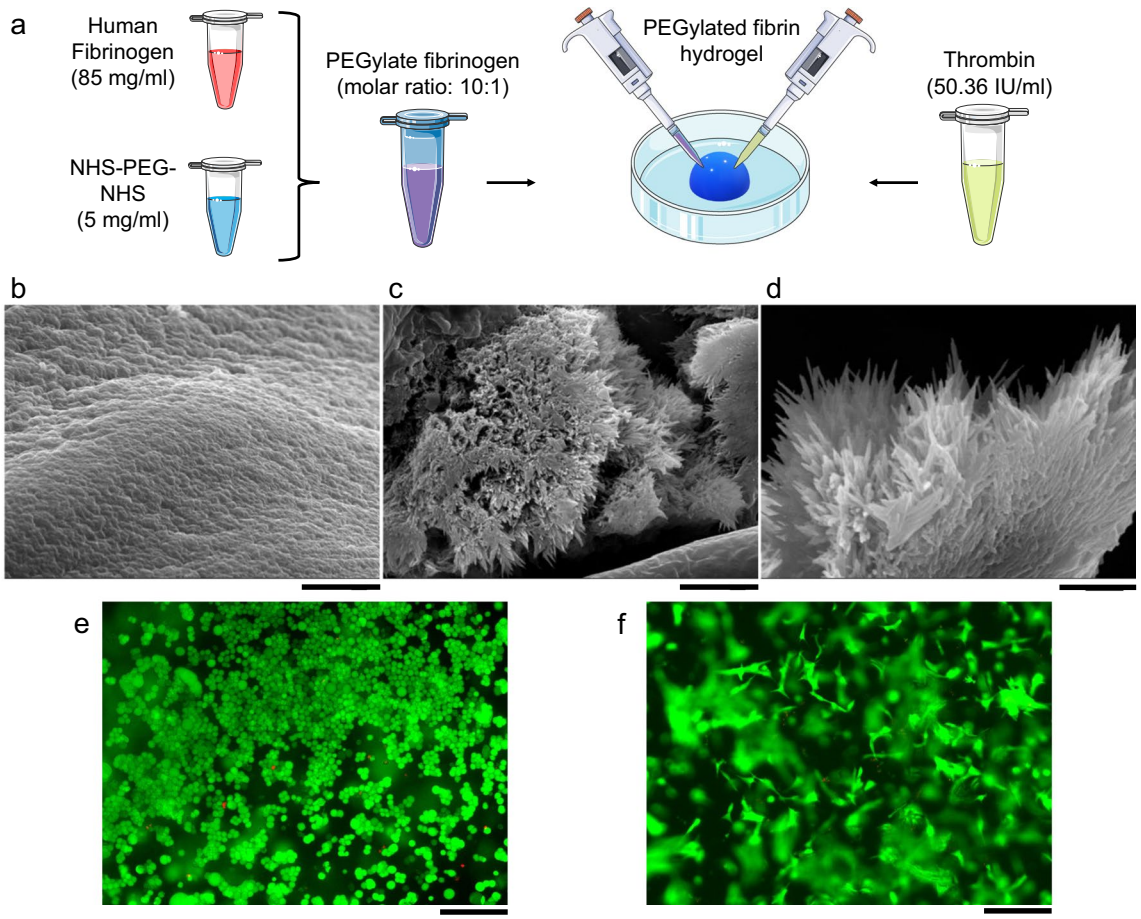

Fig. 1 Schematic illustration of the PEGylated fibrin hydrogel preparation (**a**). Representative scanning electron microscopy images of PEGylated fibrin showing surface morphology at 5000×magnification (Scale bar: 5 µm) (**b**), internal structure at 5000×magnification (Scale bar: 5 µm) (**c**), and fibers at 12,000×magnification (Scale bar: 2 µm) (**d**); The cytocompatibility of the PEGylated fibrin hydrogel containing HL-60 cells (**e**) and ovarian SCs (Scale bar: 200 µm) (**f**)

Balzers CPD030 critical point drier, coated with gold using a Leica SCD500 coater, and then examined and photographed with a Jeol JSM 7001F scanning electron microscope.

Cytocompatibility

The cytocompatibility of the PEGylated fibrin hydrogel was evaluated to ascertain that neither the hydrogel component nor the gelation process affected the viability of the embedded cells. For this purpose, 5×10^4 SCs or HL-60 cells were encapsulated in 50 µl of hydrogel and incubated in µ-slide eight-well ibiTreat dishes (80,806, Ibidi) for 24 h. Cell viability was assessed using LIVE/DEAD® cell staining (16).

TM Preparation

The mixed cells at ratios of HL-60:SCs 1:1, 1:10, 1:100, and 1:1000 were prepared after detaching SCs from flasks by Accutase and adding the appropriate volume of HL-60 cell suspensions. Afterward, mixed suspensions were centrifuged at 500 g for 5 min. PEGylated fibrinogen solution was added to different cell pellets and mixed thoroughly. The hydrogel was obtained by mixing an equal volume of the cell-suspended PEGylated fibrinogen solution and thrombin. The final cell density of SCs and HL-60 cells was 1×10^6 cells/ml for each group. 100 µL of hydrogels containing different HL-60:SCs ratios were deposited on a four-well plate (179,830; Thermo Scientific, Belgium). The hydrogels were incubated at 37°C for 15 min. After polymerization, 1 mL culture medium (containing DMEM/F12, 10% HI FBS, and 1% AA) was added to each well. The TMs were then cultured for 5 days at 37°C in a humidified incubator with 5% CO_2 ($n = 3$).

Immunofluorescence Analysis

To evaluate cell proliferation and identify cancer cells using CD43/Ki-67 practical immunofluorescence analysis, **TMs** were preserved in a 4% formaldehyde solution and embedded in paraffin before and 3 or 5 days after culture (13, 20). Sections with a 5 µm thickness were cut and placed on Superfrost Plus slides. Sections were deparaffinized and rehydrated using Histosafe and isopropanol, respectively. Following a 20-min microwave demasking step using citrate buffer and Triton X-100, the non-specific binding sites were blocked by incubating the sections for 30 min in a TBS/Tween solution containing 10% NGS and 1% BSA. The sections were subsequently treated with the polyclonal CD43 antibody (1:150) for an additional overnight at 4°C. The slides were next exposed to Alexa FluorTM 488 goat anti-mouse IgG for 40 min. The slides were then treated for 40 min with Alexa FluorTM 594 goat anti-mouse IgG and overnight at 4°C with monoclonal anti-human Ki67 (1:90). Sections were stained with Hoechst 33342 (1:500), mounted with fluorescent mounting media, and then scanned using an automated slide scanner with three laser lines of 455, 488, and 594 nm (ZEISS Axio Scan.Z1, USA). The cell density within a 200×200 µm^2 area was quantified, and the following equation was employed to assess the dynamic percentage of the cell density over 5 days (14).

$$Dynamic\ percentage\ of\ cell\ density = (CD5 - CD0)/CD5 \times 100; \quad (1)$$

Where CD5 represents the cell density on day 5, and CD0 is the cell density on day 0.

Reverse Transcription Polymerase Chain Reaction (RT-PCR)

The presence of malignant cells in **TMs** was determined using the reverse transcription polymerase chain reaction (RT-PCR) (20). The RNeasy FFPE kit (73504, Qiagen) was used to extract RNA from paraffin-embedded samples, following the manufacturer's instructions and the amount of extracted RNA was then measured using a spectrophotometer (NanoDrop 2000/2000c, Thermo Fisher Scientific). Using the goScript reverse-transcription system (A5000, Promega, Madison, WI, USA), RNA from each sample was converted into complementary DNA (cDNA) following the manufacturer's instructions and combined with TaqMan probes. SPN (Sialophorin, also known as CD43) has been chosen as a target gene for leukemia cancer cells. SPN plays a critical role in regulating hematopoietic cell function and is highly expressed in leukocytes. Its involvement in cell adhesion, migration, and immune signaling makes it a key marker for identifying leukemic cells (21). RT-PCR was performed using Applied Biosystems step-one equipment, and relative quantification values of the target genes were standardized according to the comparative threshold cycle ($2^{-\Delta\Delta CT}$).

Statistical Analysis

The quantitative data, reported as mean ± SD, were statistically examined using one-way ANOVA. P values < 0.05 were regarded as significant in statistics. The error bars in the graphs show the sample's standard deviation.

Results

Hydrogel Microstructure and Cytocompatibility

The PEGylated fibrinogen and thrombin reaction produced a dense hydrogel with a compact surface morphology (Fig. 1b). SEM analysis revealed a tightly packed fibrous network within the hydrogel structure (Fig. 1c). The fibers

exhibited an average diameter of 97 ± 25.71 nm, determined by measuring 10 distinct fibers (Fig. 1d). This tightly packed fibrous structure suggests enhanced mechanical stability and uniformity throughout the hydrogel. Furthermore, the cytocompatibility test revealed that the hydrogel exhibited no toxicity towards SCs or HL-60 cells after 24 h of embedding (Fig. 1e,f).

HL-60 and SCs Cell Density in TMs

The CD43/Ki-67 immunofluorescence double staining serves as a robust method for distinguishing between healthy and cancerous cells while simultaneously assessing cell density within hydrogels (Fig. 2a). As illustrated by the cell proportion graphs (Fig. 2b-d), distinct groups exhibited varying levels of HL-60 contamination on the third and fifth days. At day 0, a notable variance exists in the cancer cell density of TMs with an HL-60:SCs ratio of 1:1 compared to the other three groups. This contrast remains considerable for the TMs with HL-60:SCs ratios of 1:100 and 1:1000. However, the cancer cell density at an HL-60:SCs ratio of 1:10 reaches a level that is not statistically significant when compared to the 1:1 group.

The CD43/Ki-67 immunofluorescence analysis also provides insights into the dynamic changes in cell density over time. As indicated in Table I, there was no significant variation in cell density among the different groups on day 0, with all values falling within the 120–135 cells/mm^2 range. However, **TMs** with an HL-60:SCs ratio of 1:1 and 1:10 exhibited a dramatic increase in cell density by the fifth day compared to the first day. Furthermore, there were no significant differences in cell density observed between the groups with HL-60:SCs ratios of 1:100 and 1:1000 across various days of culture. However, no malignancy was detected in the **TMs** with an HL-60:SCs cell ratio of 1:1000 after five days of incubation.

Table I Cell Density Evaluation of **TMs** with Different Ratios of HL-60:SCs (1:1, 1:10, 1:100, and 1:1000) on Day 0, Day 3, and Day 5

Combination (Hl-60:SCs)	Cell density (cells per mm^2)		
	Day 0	Day 3	Day 5
1:1	129.91 ± 21.07^{a}	211.97 ± 21.07^{b}	523.08 ± 161.74^{a,b}
1:10	123.08 ± 16.75^{c}	177.78 ± 29.41^{d}	447.86 ± 49.07^{c,d}
1:100	133.33 ± 22.16	170.94 ± 37.76	215.38 ± 30.19
1:1000	129.91 ± 31.70	167.52 ± 33.84	208.55 ± 57.00

The letter in the same raw indicates the statistical difference (a-c: $p < 0.001$; d: $p < 0.01$)

Cell Density Dynamic and Proliferation Rate in TMs

The dynamic percentage of cell density reflects the changing proportion of different cell populations over time,

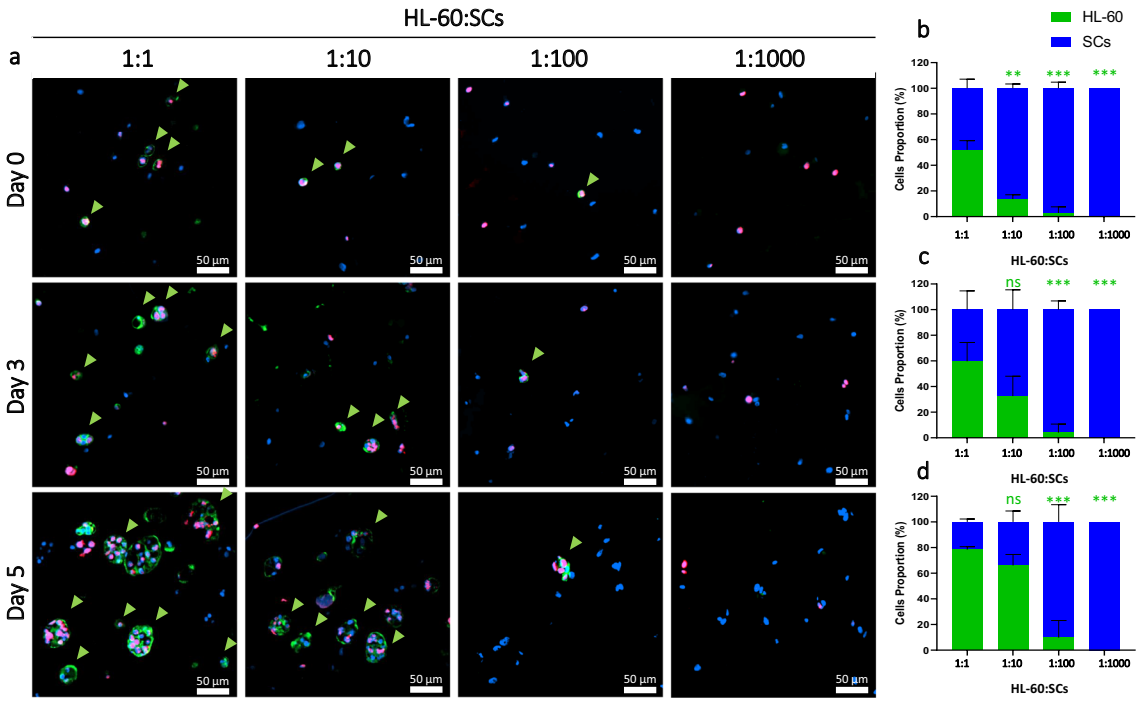

Fig. 2 CD43 (Green)/Ki67 (Red) Immunofluorescence analysis of **TMs** with different ratios of HL-60:SCs (1:1, 1:10, 1:100, and 1:1000) before and 3 or 5 days after culturing (**a**) (scale bar: 50 µm). Cell proportion evaluation on day 0 (**b**), Day 3 (**c**), and Day 5 (**d**) (ns, no significant; *, $P < 0.05$; **, $P < 0.01$; ***, $P < 0.001$)

which can significantly impact experimental outcomes by influencing cell interactions and viability. When examining the dynamics of cell density over time, TMs with ratios of 1:1 and 1:10 displayed HL-60 cell density dynamics of 82.56 ± 4.16 and 93.96 ± 2.13, respectively, after five days of incubation (Table II). However, the cell density dynamic in the groups with HL-60:SCs cell ratios of 1:1 and 1:10 was significantly higher compared to the other two groups. On the third day, in the TM group with an HL-60 to SCs ratio of 1:1, the proliferation rate of SCs was only 6.33 ± 1.96%. This rate was significantly lower than that of the fourth group, indicating that when cancer cells are utilized at an equivalent concentration as SCs, they have the potential to impact SC proliferation (Fig. 3b).

In the first two groups of cells, there was a marked increase in the HL-60 cell density after five days, with growth exceedingly sixfold compared to the initial count. Given that the HL-60 cells have a doubling time that ranges from 36 to 72 h, one would expect a cell density increase of approximately 50–75% over 3–6 days. The observed growth pattern manifested in the cohort with an HL-60 to SCs cell ratio of 1:100, whereas no malignancies were detected in the cohort with an HL-60:SCs ratio of 1:1000 on the fifth day.

Table II Cell Density Dynamics of HL-60 and SCs After 5 Days of Culturing

Combination (HL-60:SCs)	Dynamic percentage of cell density (%)		
	Total	SCs	HL-60
1:1	73.22 ± 8.10[a]	38.66 ± 13.92	82.56 ± 4.16
1:10	72.10 ± 5.06[a]	27.78 ± 12.86	93.96 ± 2.13
1:100	36.44 ± 14.86[b]	32.96 ± 5.00	66.67 ± 47.14
1:1000	37.17 ± 2.72[b]	37.17 ± 2.72	-

The *p*-value for the statistical difference between the letters a and b is less than 0.05

Tumor-Specific Gene Expression in TMs

While the immunohistochemical analysis is a strong tool to distinguish malignant cells and their proliferation at the same time, it depends on the sectioning and in the case of malignancy search in the tissue it can be challenging to rely. Tumor-specific gene expression is an exciting tool to search the precense of malignant cells in the **TMs** quickly and thoroughly (20). In this study, the expression of sialophorin (CD43), a sialoglycoprotein expressed on human neoplastic hematopoietic cell lines, including HL-60, was chosen as the gene that specifically detects the tumor inside the **TMs** on different days (Fig. 4).

When the expression level of different groups was quantified and normalized to the endogenous control (Fig. 5), it confirmed the immunohistochemical results. A notable increase in the tumor gene level was observed in the **TMs** groups with HL-60:SCs ratios of 1:1 and 1:10. Interestingly, the gene expression levels for **TMs** with an HL-60:SCs ratio of 1:100 remained relatively stable, while still being detectable throughout the culture period.

Discussion

Hydrogel-based biomaterials have proven to be highly effective in developing tumor models for various cancer types, such as prostate, ovarian, and pancreatic cancer (22–24). To create engineered tumor microenvironments, different natural and synthetic hydrogel materials have been used as 3D artificial tumor microenvironments that can provide mechanical support while regulating tumor behaviors within the matrix. In this study, we selected fibrin as the biomaterial for creating tissue constructs. This FDA-approved biomaterial exhibits biocompatibility and biodegradability and enhances cell adhesion and proliferation by providing a biomimetic extracellular matrix. Furthermore, it facilitates the formation of a capillary network (25). To improve protein stability and protect against proteolytic activity, we utilized PEGylation.

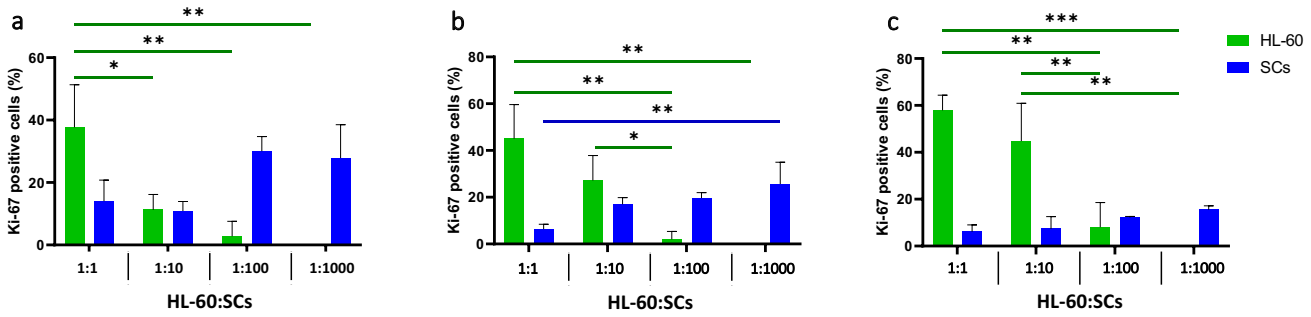

Fig. 3 Proliferative HL-60 and SCs before culturing (**a**) and after 3 (**b**) or 5 (**c**) days of culturing (ns, no significant; *, $P<0.05$; **, $P<0.01$; ***, $P<0.001$)

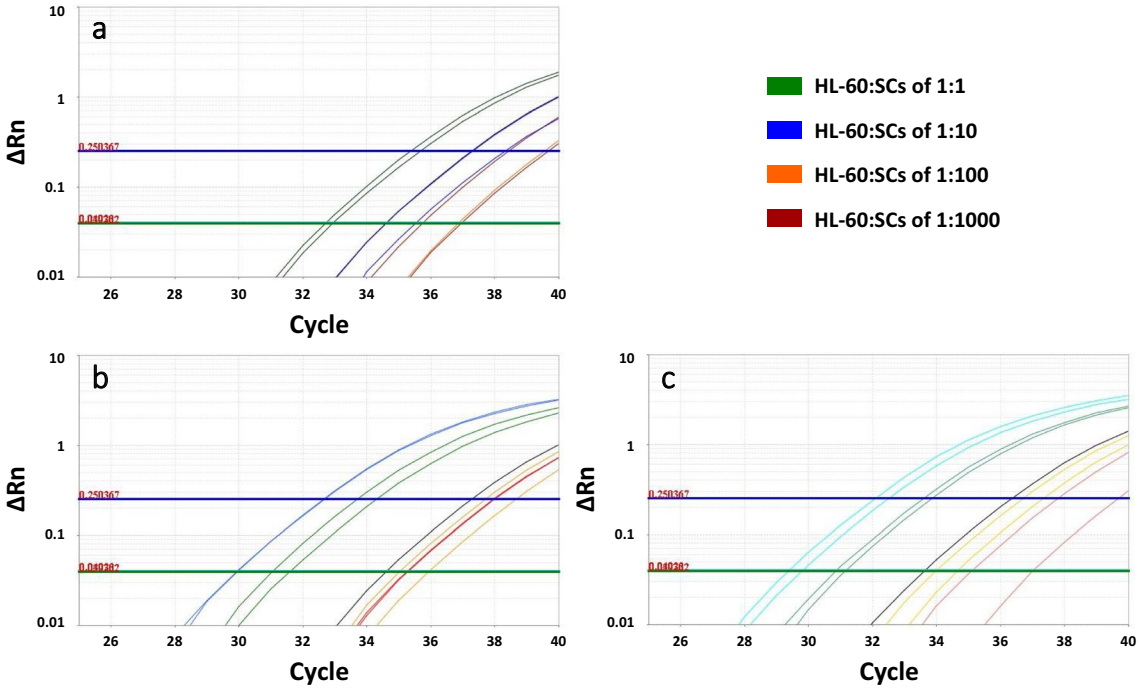

Fig. 4 RT-PCR analysis showing the tumor-specific gene expression in **TMs** with different ratios of HL-60:SCs (1:1, 1:10, 1:100, and 1:1000) before (**a**) and 3 (**b**) or 5 (**c**) days after culturing

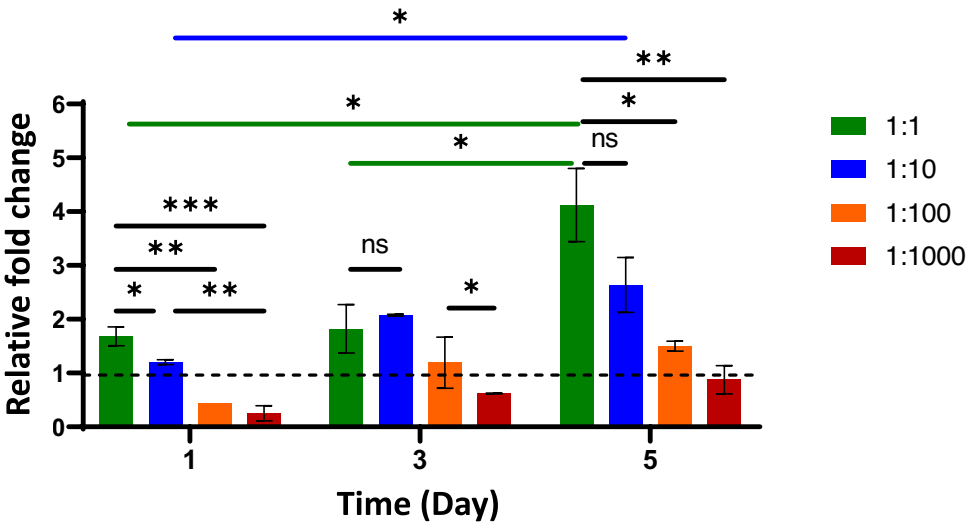

Fig. 5 Quantified fold change relative gene expression in **TMs** with different ratios of HL-60:SCs (1:1, 1:10, 1:100, and 1:1000), normalized to the endogenous control (ns, no significant; *, $P<0.05$; **, $P<0.01$; ***, $P<0.001$)

Thrombin in the medium polymerizes PEGylated fibrinogen by cleaving fibrinogen, while Ca2 + in the scaffold further stabilizes the hydrogel network (26). PEGylated fibrin hydrogels have been successfully employed in tumor models, such as human lung adenocarcinoma, reducing the need for complex animal models and addressing limitations associated with xenografting techniques (12). In another study, PEGylated fibrin hydrogels were used to create breast cancer tumor models, demonstrating high cell viability and significant cell spreading and growth (27). In our previous study, we developed an engineered scaffold for an artificial ovary using PEGylated fibrin hydrogel, optimizing its formulation to replicate Young's modulus of the human ovarian cortex at reproductive age (28). Indeed, the mechanical properties of a scaffold are critical in influencing cellular behaviors, including migration speed, proliferation, differentiation, and attachment. When a scaffold accurately mimics the mechanical characteristics of natural tissue, it can effectively guide cells to respond in ways that mirror their behavior in the native environment (29, 30). Therefore, we applied the

optimized PEGylated fibrin hydrogel to develop TMs that closely replicate the architecture of invasive leukemia within healthy ovarian tissue. This scaffold demonstrated excellent structural stability and effectively supported cell viability and proliferation, making it an ideal platform for replicating the organization and function of natural tissues.

AML is characterized by its heterogeneous nature, presenting a range of variations. Despite this complexity, established cell lines have proven invaluable in the field for many years. They offer a robust platform for systematic, reproducible, and cost-efficient studies. These leukemia cells are mainly found in bodily fluids rather than forming solid tumors (31, 32). Interestingly, HL-60 cells have shown an ability to spontaneously develop colonies in semi-solid environments (33, 34). In this study, it is crucial to carefully adjust the ratio of HL-60 to SCs to achieve a delicate balance. This balance aims to avoid excessive solid tumor formation while maintaining sufficient malignancy levels for a meaningful model.

The findings from our study reveal a significant influence of cellular ratio on HL-60 cell proliferation and invasion potential. When cancer cells are used at an equivalent concentration to SCs, they can significantly impact SC proliferation. This influence is likely due to nutrient competition, as myeloid cells are known to consume notably high glucose levels. Additionally, paracrine signaling and metabolic byproducts produced by the cancer cells may contribute to this effect (35). Moreover, at the 1:1 and 1:10 HL-60:SCs ratios, we observed a marked increase in proliferation rates compared to the Day 0 measurements. The observed proliferation in these two groups was likely influenced by external factors such as differences in the microenvironment and cell–cell interactions. These findings may have far-reaching implications for interpreting experimental data in which cell growth is critical, potentially impacting research areas such as cancer biology, drug development, and tissue engineering. At lower cell ratios, such as 1:100, the limited number of HL-60 cells may not receive sufficient signaling cues to trigger substantial proliferation. Therefore, they demonstrated enhanced capability in mimicking the invasion of leukemia cells into ovarian tissue. This was evident as their malignancy remained detectable even after 5 days of *in vitro* culture, with no significant alterations in cell density and cell density dynamics. The absence of cancer cells in the fourth group may be attributed to the suppressive effect of mesenchymal stem cells (MSCs) within the isolated ovarian SCs (36) on neighboring malignant leukemia cells (37, 38). MSCs are known to possess immunomodulatory and anti-tumor properties, which have been documented in several studies. These cells can inhibit tumor growth by secreting various cytokines and chemokines, which modulate the immune response and potentially induce apoptosis in malignant cells (39). Given the evidence from our earlier characterization of the ovarian SCs, which demonstrated the presence of MSC-like cells, it is plausible that these MSCs contributed to the inhibition of leukemia cell proliferation in the fourth group (40). Recently, Jalilivand *et al*. (41) demonstrated that exosomes released from bone-marrow MSCs can significantly repress metabolic activity, proliferation, and cell cycle progression in HL-60 leukemic cells, increasing apoptosis and enhancing the ROS index. Further investigation is imperative to elucidate the specific mechanisms underlying the observed differences in cell growth between these experimental groups. This may entail a comprehensive exploration of gene expression profiles, signaling pathways, and microenvironmental cues.

Conclusion

In conclusion, our study successfully established a 3D tumor microenvironment that closely mimics the complex dynamics of leukemia invasion within healthy ovarian tissue. The PEGylated fibrin hydrogel scaffold we developed provides a robust and stable platform supporting cell viability and proliferation, demonstrating its potential for engineered tissue models.

Our findings highlight the critical role of the HL-60 cells and SCs ratio in influencing key processes such as cell proliferation, tumor formation, and invasion. At higher cancer cell concentrations, competition for nutrients and enhanced cell–cell interactions appear to drive HL-60 cell proliferation. Conversely, lower cancer cell ratios allow for more accurate modeling of leukemia cell invasion into ovarian tissue. Interestingly, the observed suppression of cancer cells in certain groups suggests that MSCs within the ovarian SCs population may exert significant anti-tumor effects through immunomodulatory mechanisms, leading to the suppression of cancer cell growth. These findings suggest that MSCs could play a crucial role in controlling tumor progression within the ovarian microenvironment.

Future research should focus on further unraveling the mechanisms driving these observations, particularly the influence of cell ratios on tumor behavior. Gaining a comprehensive understanding of the mechanisms underlying the changes in the rate of cell growth in TMs with varying cell ratios has the potential to not only improve the accuracy of interpreting experimental data but also provide valuable insights for the development of targeted interventions and therapies. Overall, this work has important implications for advancing our understanding of cancer biology, supporting drug development, and improving tissue engineering approaches. By exploring the interplay between cell ratios, the tumor microenvironment, and cellular interactions, this study contributes valuable knowledge to develop more precise and effective therapeutic strategies.

Author Contributions Conceptualization, formal analysis, investigation, and writing—original draft preparation, A.D., and S.M., investigation C.M.L., writing—review, editing, and supervision, C.A.A.

Funding This study was supported by grants from the Fonds National de la Recherche Scientifique (FNRS-PDR Convention grant number T.0004.20 awarded to C.A.A. and FC 46825 awarded to S.M.).

Data Availability Data will be made available on request.

Declarations

Conflicts of Interest The authors declare that they have no known competing financial interests or personal relationships that could have appeared to influence the work reported in this paper.

References

1. Fitzgerald KA, Malhotra M, Curtin CM, O'Brien FJ, O'Driscoll CM. Life in 3D is never flat: 3D models to optimise drug delivery. J Control Release. 2015;215:39–54.
2. Saglam-Metiner P, Gulce-Iz S, Biray-Avci C. Bioengineering-inspired three-dimensional culture systems: Organoids to create tumor microenvironment. Gene. 2019;686:203–12.
3. Szot CS, Buchanan CF, Freeman JW, Rylander MN. 3D in vitro bioengineered tumors based on collagen I hydrogels. Biomaterials. 2011;32(31):7905–12.
4. Monteiro MV, Gaspar VM, Ferreira LP, Mano JF. Hydrogel 3D in vitro tumor models for screening cell aggregation mediated drug response. Biomater Sci. 2020;8(7):1855–64.
5. Song H-HG, Park KM, Gerecht S. Hydrogels to model 3D in vitro microenvironment of tumor vascularization. Adv Drug Deliv Rev. 2014;79:19–29.
6. Knowlton S, Onal S, Yu CH, Zhao JJ, Tasoglu S. Bioprinting for cancer research. Trends Biotechnol. 2015;33(9):504–13.
7. Vilaplana-Lopera N, Cuminetti V, Almaghrabi R, Papatzikas G, Rout AK, Jeeves M, et al. Crosstalk between AML and stromal cells triggers acetate secretion through the metabolic rewiring of stromal cells. Elife. 2022;11:e75908.
8. Forte D, García-Fernández M, Sanchez-Aguilera A, Stavropoulou V, Fielding C, Martín-Pérez D, et al. Bone marrow mesenchymal stem cells support acute myeloid leukemia bioenergetics and enhance antioxidant defense and escape from chemotherapy. Cell Metabol. 2020;32(5):829-43.e9.
9. Kouzi F, Zibara K, Bourgeais J, Picou F, Gallay N, Brossaud J, et al. Disruption of gap junctions attenuates acute myeloid leukemia chemoresistance induced by bone marrow mesenchymal stromal cells. Oncogene. 2020;39(6):1198–212.
10. Pampaloni F, Reynaud EG, Stelzer EH. The third dimension bridges the gap between cell culture and live tissue. Nat Rev Mol Cell Biol. 2007;8(10):839–45.
11. Bharadwaj AG, Holloway RW, Miller VA, Waisman DM. Plasmin and plasminogen system in the tumor microenvironment: implications for cancer diagnosis, prognosis, and therapy. Cancers. 2021;13(8):1838.
12. Del Bufalo F, Manzo T, Hoyos V, Yagyu S, Caruana I, Jacot J, et al. 3D modeling of human cancer: A PEG-fibrin hydrogel system to study the role of tumor microenvironment and recapitulate the in vivo effect of oncolytic adenovirus. Biomaterials. 2016;84:76–85.
13 Dadashzadeh A, Moghassemi S, Peaucelle A, Lucci CM, Amorim CA. Mind the mechanical strength: tailoring a 3D matrix to encapsulate isolated human preantral follicles. Hum Reprod Open. 2023;2023(2):hoad004.
14. Dadashzadeh A, Moghassemi S, Amorim C. Evaluation of PEGylated fibrin as a three-dimensional biodegradable scaffold for ovarian tissue engineering. Mater Today Chem. 2021;22:100626.
15. Moghassemi S, Dadashzadeh A, Camboni A, Feron O, Azevedo RB, Amorim CA. Photodynamic therapy using OR141-loaded nanovesicles for eradication of leukemic cells from ovarian tissue. Photodiagn Photodyn Ther. 2022;40:103139.
16. Moghassemi S, Dadashzadeh A, de Souza PEN, Azevedo RB, Amorim CA. AlPc/ZnPc-based oncological photodynamic therapy for a selective eradication of leukemic cells from ovarian tissue. Photodiagn Photodyn Ther. 2021;36:102555.
17. Moghassemi S, Dadashzadeh A, de Azevedo RB, Amorim CA. Secure transplantation by tissue purging using photodynamic therapy to eradicate malignant cells. J Photochem Photobiol B. 2022;234:112546.
18. Dadashzadeh A, Moghassemi S, Grubliauskaité M, Vlieghe H, Brusa D, Amorim CA. Medium supplementation can influence the human ovarian cells in vitro. J Ovarian Res. 2022;15(1):1–12.
19 Amorim CA, Dolmans M-M, David A, Jaeger J, Vanacker J, Camboni A, et al. Vitrification and xenografting of human ovarian tissue. Fertil Steril. 2012;98(5):1291-8. e2.
20 Moghassemi S, Dadashzadeh A, Camboni A, Feron O, Azevedo RB, Amorim CA. Ex vivo purging of cancer cells from ovarian tissue using photodynamic therapy: a novel strategy to restore fertility in leukemia patients. Hum Reprod Open. 2023;2023(2):hoad005.
21 Bruveris FF, Ng ES, Leitoguinho AR, Motazedian A, Vlahos K, Sourris K, et al. Human yolk sac-like haematopoiesis generates RUNX1-, GFI1-and/or GFI 1B-dependent blood and SOX17-positive endothelium. Development. 2020;147(20):dev193037.
22. Braccini S, Tacchini C, Chiellini F, Puppi D. Polymeric hydrogels for in vitro 3D ovarian cancer modeling. Int J Mol Sci. 2022;23(6):3265.
23. Piłat E, Kurdyn A, Kucińska-Lipka J. Naturally-derived hydrogels for 3D pancreatic tumor models: A short review. Polym Renewable Resour. 2023;14(4):279–88.
24. Tang Y, Huang B, Dong Y, Wang W, Zheng X, Zhou W, et al. Three-dimensional prostate tumor model based on a hyaluronic acid-alginate hydrogel for evaluation of anti-cancer drug efficacy. J Biomater Sci Polym Ed. 2017;28(14):1603–16.
25. Dadashzadeh A, Moghassemi S, Shavandi A, Amorim CA. A review on biomaterials for ovarian tissue engineering. Acta Biomater. 2021;135:48–63.
26. Galler KM, Cavender AC, Koeklue U, Suggs LJ, Schmalz G, D'Souza RN. Bioengineering of dental stem cells in a PEGylated fibrin gel. Regen Med. 2011;6(2):191–200.
27. Pradhan S, Hassani I, Seeto WJ, Lipke EA. PEG-fibrinogen hydrogels for three-dimensional breast cancer cell culture. J Biomed Mater Res, Part A. 2017;105(1):236–52.
28. Moghassemi S, Dadashzadeh A, Amorim CA. A novel bioprinted microtumour model for studying acute-leukemia-cell-contaminated in ovarian tissue. Life Sci. 2024;355:122992.
29. Vedadghavami A, Minooei F, Mohammadi MH, Khetani S, Kolahchi AR, Mashayekhan S, Sanati-Nezhad A. Manufacturing of hydrogel biomaterials with controlled mechanical properties for tissue engineering applications. Acta Biomater. 2017;62:42–63.
30. Ghosh K, Pan Z, Guan E, Ge S, Liu Y, Nakamura T, et al. Cell adaptation to a physiologically relevant ECM mimic with different viscoelastic properties. Biomaterials. 2007;28(4):671–9.
31. Ohanian M, Faderl S, Ravandi F, Pemmaraju N, Garcia-Manero G, Cortes J, Estrov Z. Is acute myeloid leukemia a liquid tumor? Int J Cancer. 2013;133(3):534–43.
32 Zhu Z, Hattori K, Zhang H, Jimenez X, Ludwig D, Dias S, et al. Inhibition of human leukemia in an animal model with human

antibodies directed against vascular endothelial growth factor receptor 2. Correlation between antibody affinity and biological activity. Leukemia. 2003;17(3):604–11.
33. Spangelo BL, Pompilius M, Farrimond DD, Stevens N, Nieva R, Shroff S, et al. Presence of a peptide component of thymosin fraction-5 manifesting discrete cytostatic properties in HL-60 human promyelocytic leukemia cells. Int Immunopharmacol. 2005;5(7–8):1317–29.
34. Skopek R, Palusińska M, Kaczor-Keller K, Pingwara R, Papierniak-Wyglądała A, Schenk T, et al. Choosing the right cell line for acute myeloid leukemia (AML) research. Int J Mol Sci. 2023;24(6):5377.
35. Liesveld JL, Rosell KE, Lu C, Bechelli J, Phillips G II, Lancet JE, Abboud CN. Acute myelogenous leukemia—microenvironment interactions: role of endothelial cells and proteasome inhibition. Hematology. 2005;10(6):483–94.
36. Vlieghe H, Sousa MJ, Charif D, Amorim CA. Unveiling the differentiation potential of ovarian theca interna cells from multipotent stem cell-like cells. Cells. 2024;13(15):1248.
37. Cetintas VB, Aktug H, Oltulu F, Keskinoglu A, Del Castello BE, Taskiran D. The effects of mesenchymal stem cells on lymphoblastic leukemia cell proliferation. J BUON. 2014;19(4):1006–17.
38. Moghassemi S, Dadashzadeh A, Sousa MJ, Vlieghe H, Yang J, León-Félix CM, Amorim CA. Extracellular vesicles in nanomedicine and regenerative medicine: A review over the last decade. Bioactive Mater. 2024;36:126–56.
39. Eiro N, Fraile M, Fernández-Francos S, Sánchez R, Costa LA, Vizoso FJ. Importance of the origin of mesenchymal (stem) stromal cells in cancer biology:“alliance” or “war” in intercellular signals. Cell Biosci. 2021;11(1):109.
40. Dadashzadeh A, Moghassemi S, Grubliauskaité M, Vlieghe H, Brusa D, Amorim CA. Medium supplementation can influence the human ovarian cells in vitro. J Ovarian Res. 2022;15(1):137.
41. Jalilivand S, Izadirad M, Vazifeh Shiran N, Gharehbaghian A, Naserian S. The effect of bone marrow mesenchymal stromal cell exosomes on acute myeloid leukemia's biological functions: a focus on the potential role of LncRNAs. Clin Exp Med. 2024;24(1):1–15.